Open Access Journal

Journal of Power Technologies 97 (4) (2017) 272–282

journal homepage:papers.itc.pw.edu.pl

Power Quality Enhancement in Hybrid Photovoltaic-Battery System based on three–Level Inverter associated with DC bus Voltage Control

Belkacem Belabbas*, Tayeb Allaoui, Mohamed Tadjine, Mouloud Denai

Laboratory of L2GEGI, University of Tiaret, 14000, Algeria

Abstract

This modest paper presents a study on the energy quality produced by a hybrid system consisting of a Photovoltaic (PV) power source connected to a battery. A three-level inverter was used in the system studied for the purpose of improving the quality of energy injected into the grid and decreasing the Total Harmonic Distortion (THD). A Maximum Power Point Tracking (MPPT) algorithm based on a Fuzzy Logic Controller (FLC) is used for the purpose of ensuring optimal production of photovoltaic energy. In addition, another FLC controller is used to ensure DC bus stabilization. The considered system was implemented in the Matlab /Simpower environment. The results show the effectiveness of the proposed inverter at three levels in improving the quality of energy injected from the system into the grid.

Keywords: Power quality; Photovoltaic; Battery; Three-level inverter; Fuzzy logic control

1. Introduction

Global interest in clean and renewable energy sources (RESs) has been growing exponentially. Solar energy is gaining in importance as a renewable source due to advantages such as low maintenance, no noise, no fuel cost, and low wear and tear due to the absence of moving parts [1–6]. The energy conversion efficiency of a PV array is low and varies with solar intensity and operating temperature [7]. The tracking control of the maximum power point is a key and complex issue. Therefore, to achieve the maximum efficiency possible, Maximum Power Point Tracking (MPPT) control is critical to the success of PV systems. To mitigate the problems involved, various tracking control strategies have been discussed in past literature with a view to obtaining maximum energy conversion efficiency of the PV array for all operation conditions, such as perturb and observe [3, 8] and incremental conductance [8–11]. These strategies have disadvantages such as difficulty, high cost, instability and complexity. To overcome these disadvantages, several researchers have used artificial intelligence approaches such as Fuzzy Logic Controller (FLC) [6, 12–17] and Artificial Neural Network (ANN) [18–22] to obtain maximum energy conversion efficiency. This study discusses the FLC method to deliver MPPT for a PV system. Fuzzy logic is robust and relatively simple to design, since it does not require information about the exact model or load level. Another element that plays a very important role in solar generation power systems is battery storage [2, 17, 23–25]. Batteries are used to store superfluous energy derived from solar irradiance on sunny days and for release on cloudy days or at night. Battert technology has made considerable advances, the rechargeable battery has been upgraded from a lead acid battery to a nickel-based battery and from a nickel-based battery to a lithium-ion (Li-ion) battery [26]. Nowadays, Li-ion batteries are widely adopted in portable electronic devices, such as smart phones, digital cameras and laptop computers. Lithium-ion batteries enjoy higher energy density, higher terminal voltage and higher power density than other rechargeable batteries [23, 27–29]. This study integrated a PV system with a Li-ion battery charging system connected to the grid via a three-level neutral point clamp (NPC) inverter. Multilevel converters are considered to be the most suitable power converters in renewable energy applications, especially in developing high-power generators [6, 25]. Multilevel converters present many advantages when compared with the standard two-level conventional converters, such as improved output voltage waveform, reduced harmonic content, increased power rating, and decreased stress across the switches. However, their main disadvantage is the balancing of the capacitor voltages in the DC link [3, 30]. The operation of a PV-Battery system with a three level NPC in-

*Corresponding author

Email addresses: belabbas_1986@yahoo.fr (Belkacem Belabbas), allaoui.tayeb@univ-tiaret.dz (Tayeb Allaoui), mohamed.tadjine@mail.enp.edu.dz (Mohamed Tadjine), m.denai@herts.ac.uk (Mouloud Denai)

verter was presented by researchers in [3–6, 25, 31–34]. In [3, 5, 31, 32, 34, 35], the authors present a PV unti connected to the grid through a three-level NPC inverter without a battery system. However, in [5, 31, 32] the system control of DC voltage, power quality and the method of MPPT are not discussed, in [3, 33, 34] the authors used the classical MPPT and in Ref [35] the complete system control is not discussed whereas power quality (THD) is very important for a system using a three-level NPC inverter. In [25] the authors present a PV-battery system connected to the grid through a five-level inverter. However, system control of DC voltage is not discussed or the use of the classical MPPT. In [6] the authors proposed a PV array connected to the grid through a three-level NPC inverter using a fuzzy controller for MPPT. However, in [6] the authors did not use a battery.

In this paper, a hybrid PV-Battery system connected to the grid via a three level NPC inverter is developed to meet the following objectives:

- FLC to track the maximum power from PV.
- Effective control coordination among PV, battery, load and the grid.
- Proposed three-level NPC inverter designed with the aim of transferring energy produced from PV arrays to the grid and to helps to reduce the THD from current injected to the grid.
- Proposed use of a lithium-ion battery to store or supply energy and to stabilize the voltage of DC bus against fluctuations.
- Stability between energy produced and energy supplied.
- Improved power quality with THD lower than 5%.
- Proposed control scheme of DC voltage consisting of two loops: the outer closed loop controls the average value of the DC voltage with FLC, whereas the inner loop controls the difference between the two voltages in each half-arm using a clamping bridge circuit.

The paper is organized as follows: Section 2 describes the proposed PV/battery system. The modeling and control of the NPC three level inverters are developed and explained in Section 3. Supervisory Control System is presented in Section 4. The simulation results are presented in Section 5 and finally discussions and conclusions are given in Section 6.

2. Modeling of the PV-Battery System

The proposed grid-connected PV-battery system is shown in Fig. 1. The PV array is connected to the DC bus via a boost converter controlled by a MPPT algorithm to extract the maximum power. The DC bus is then connected to the AC bus through the NPC three-level inverter. The battery is connected to the DC link through a DC-DC bidirectional converter and contributes to the regulation of the DC link voltage

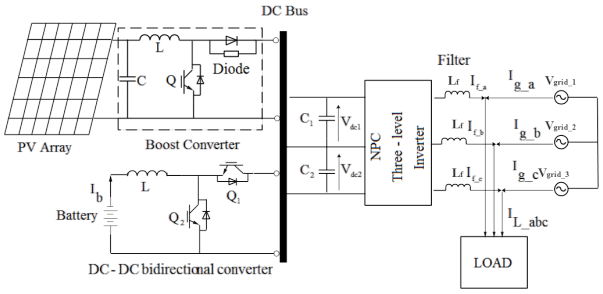

Figure 1: PV-Battery power system connected to the grid

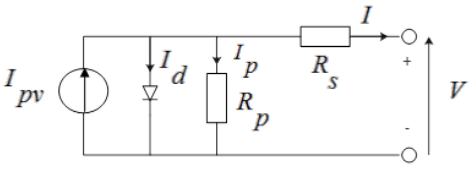

Figure 2: Single-diode equivalent circuit of a PV cell

and to power balance the supply and demand of power. A small L- filter is connected with the inverter output to eliminate high frequency harmonics.

2.1. Modeling of the PV System and Design of MPPT Control Strategy

2.1.1. PV array model

The electric power generated from the PV array fluctuates with the operating conditions and field factors such as the sun's position angle, irradiation levels and ambient temperature. A solar cell can be represented as a current source model, as shown in Fig. 2.

Applying Kirchhoff's current law, the terminal current of the cell is [4, 24]:

$$I = I_{pv} - I_d - I_p \tag{1}$$

$$I_p = \frac{V + R_s I}{R_p} \tag{2}$$

The junction current is given by:

$$I_d = I_0 \left[e^{\left(\frac{V+R_s I}{V_t \alpha}\right)} - 1 \right] \tag{3}$$

The formula relating the current and voltage in the circuit is:

$$I = I_{pv} - I_0 \left[e^{\left(\frac{V+R_s I}{V_t \alpha}\right)} - 1 \right] - \frac{V + R_s I}{R_p} \tag{4}$$

$$V_t = \frac{N_s K T}{q} \tag{5}$$

The light generated current of the PV cell depends linearly on the solar irradiation and is also influenced by the temperature according to the following equation [4, 6, 7, 24, 25]:

$$I_{pv} = \left(I_{pv,n} + K_I \Delta_T \right) + \frac{G}{G_n} \tag{6}$$

Table 1: Proposed system parameters

Parameters of the model of the PV	
Type	KC200GT
$P_{max,n}$, W	200.143
$V_{oc,n}$, V	32.9
$I_{sc,n}$, A	8.21
$I_{0,n}$, A	$9.825 \cdot 10^{-8}$
R_p, Ω	415.405
R_s, Ω	0.221
K_v, V/K	-0.123
K_I, A/K	0.0032
a	1.3
N_s	54
DC/DC converter parameters	
Chopper type	Boost
Semiconductor switch type	IGBT
Converter inductor, μH	11
Converter capacitor, mF	1
Battery	
Battery type	Lithium-ion
Nominal voltage, V	120
Capacity rating, Ah	50
Nominal discharge current, A	21.7391
Bidirectional DC/DC converter parameters	
Chopper type	Buck-Boost
Semiconductor switch type	IGBT
Converter inductor, mH	75
Converter capacitor, μF	2200
DC link voltage, V	600
Three level NPC Inverter	
Semiconductor switch type	IGBT/DIODE
Snubber resistance, Ω	1e5
Snubber capacitor	Inf
Internal resistance, mΩ	1e-3
Sampling period, μS	1
Frequency, Hz	50

The diode saturation current and its dependence on the temperature may be expressed by:

$$I_0 = \frac{I_{sc,n} + K_I \Delta_T}{\left(\frac{I_{oc,n}+K_V \Delta_T}{\alpha V_t}\right) - 1} \tag{7}$$

The parameters and model constants of the KC200GT solar array, used in this study, are given in Table 1.

2.1.2. Maximum Power Point Tracking (MPPT)

Fig. 3 shows the basic circuit configuration of a DC-DC boost converter with an MPPT controller. A capacitor is generally connected between PV panel and the boost circuit to reduce high frequency harmonics [36].

MPPT algorithms have been proposed to automatically find the PV panel operating voltage that produces the maximum power output. Several MPPT techniques exist in the literature ranging from the simplest methods such as Perturb & Observe [3, 8] and Incremental Conductance [8, 9] to more sophisticated and complex ones. In this paper, an MPPT algorithm based on fuzzy logic control (FLC) is proposed. Similar FLC-based MPPT controllers were proposed in [6, 17]. The basic scheme of a FLC is shown in Fig. 4. The inputs are the error E and error change dE; the output is the PWM duty cycle variation dD.

Where K_E, K_{dE} and K_{dD} are scaling gains selected to achieve the desired transient and steady-state response

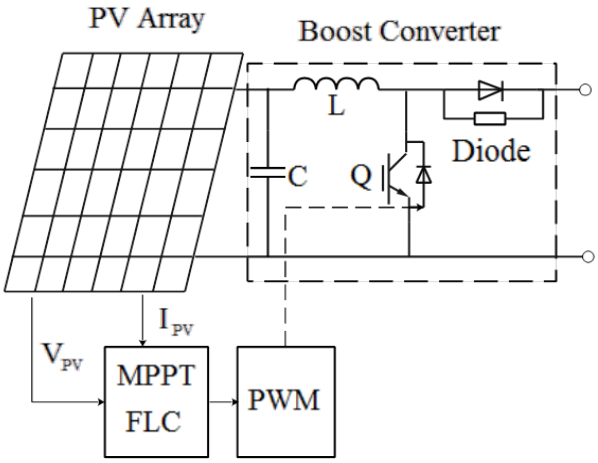

Figure 3: Boost converter circuit and MPPT control

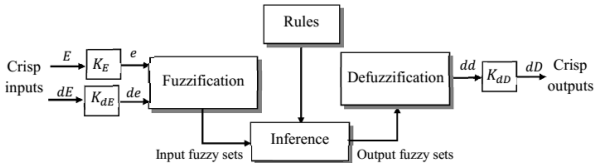

Figure 4: Building blocks and structure of a FLC

characteristics [6, 12–14, 16]. The universe of discourse for each input and output variable is divided into three fuzzy sets defined by triangular membership functions and labelled as NS (Negative Small), Z (Zero) and NB (Negative Big) as shown in Fig. 5. The fuzzy rules used to determine the controller output are summarized in Table 2. The defuzzification is based on the popular center of gravity method.

2.2. Battery Energy Storage System (BESS)

2.2.1. Li-Ion Battery Model

The modeling approach is based on the equivalent circuit of the battery shown in Fig. 6. Where R represents the conducting resistance and the resistance from leading wires, $R1$ and $C1$ represent effects caused by mass transport, $R2$ and $C2$ represent effects caused by the charge transfer and the electrochemical double layer. The model will therefore include a State of Charge (SOC) controlled voltage source and its equivalent impedance [23, 26, 27, 37].

2.2.2. Battery Control System

The objective of the control system is to regulate the battery current in order to obtain the required power. Charging

Table 2: Fuzzy Control Rule Table

dE \ E	NS	Z	NB
NS	NS	NS	Z
Z	NS	Z	NB
NB	Z	NB	NB

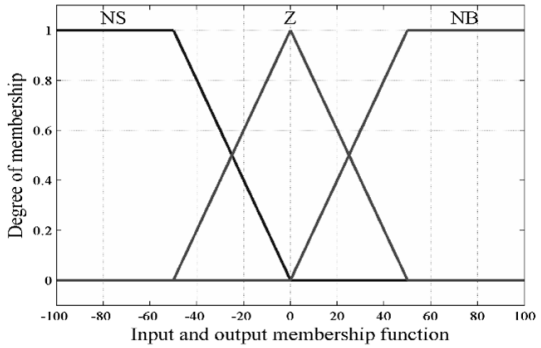

Figure 5: Fuzzy membership functions for the input and output variables

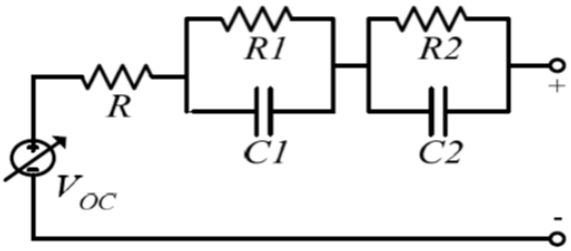

Figure 6: Equivalent circuit based Li-ion battery model

and discharging current limits and maximum SOC limitations are also included in the model. The BESS is connected to the DC grid via a bi-directional Buck-Boost DC/DC converter, as shown in Fig. 7. The BESS will operate in charging, discharging or floating modes depending on the energy requirements and these modes are managed according to the DC bus voltage at the BESS point of coupling. Consequently, the BESS is required to provide necessary DC voltage level under different operating modes of the microgrid. When charging, switch Q_2 is activated and the converter works as a boost circuit; otherwise, when discharging, switch Q_1 is activated and the converter works as a buck circuit. When the voltage at the DC link is lower than the voltage reference, switch Q_1

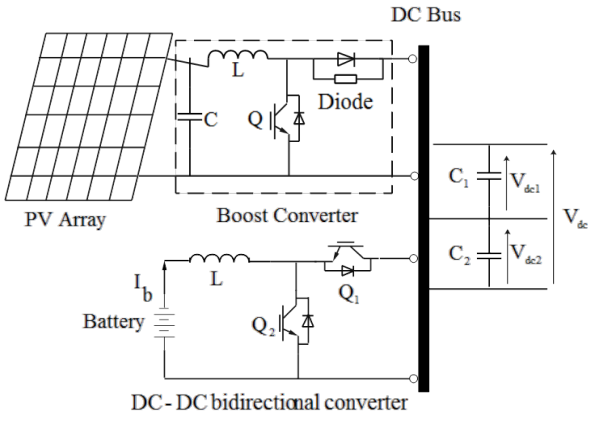

Figure 7: Battery with bi-directional buck-boost DC/DC converter

is activated. Alternatively, when the voltage at the DC link is higher than the voltage reference, switch Q_2 is activated. The PV-battery system response to transient variations is characterized by an inherent time constant. In such cases, capacitors along the DC grid can act as virtual inertia to supply the shortfall or absorb the surplus of energy [2, 25, 29, 38, 39]. The DC-link power balance can be expressed by the following differential equation:

$$V_{dc} i_{dc} = P_{PV} + P_{bat} - P_{Load} \tag{8}$$

Neglecting the losses in the power converters, battery, filtering inductors and transformer and also the harmonics due to switching actions, the power balance of the integrated hybrid distributed generation system (DGS) with energy storage is governed by:

$$V_{dc} i_{dc} = C V_{dc} \frac{dV_{dc}}{dt} = P_{PV} + P_{bat} - P_{Load} \tag{9}$$

The objective of the battery converter is to maintain constant voltage at the DC link, so the ripple in the capacitor voltage is much lower than the steady-state voltage.

If the powers injected by the two back-to-back voltage source converters (VSC) are assumed constant at any particular instant, the power from the battery is responsible for adjusting the capacitor voltage. Therefore, the transfer function from P_{pv} to V_{dc} is given by:

$$\frac{V_{dc}(s)}{P_{bat}(s)} = \frac{1}{C V_{dc} s} \tag{10}$$

Considering that the battery voltage remains constant at any instant:

$$P_{bat} = V_{bat} i_{bat} \tag{11}$$

Equation (11) becomes

$$\frac{V_{dc}(s)}{i_{bat}(s)} = \frac{V_{bat}}{C V_{dc} s} \tag{12}$$

Equation (12) suggests that linear first-order dynamics exist between the battery current and the DC link voltage. Therefore, the reference value of i_{bat} can be generated using a voltage feedback control loop based on an FLC controller as follows.

$$i^*_{bat} = (FLC)\left(V^*_{dc} - V_{dc}\right) \tag{13}$$

$$V_{dc} = \frac{V_{dc1} + V_{dc2}}{2} \tag{14}$$

The FLC used here is similar to the one used in the MPPT, which will be presented in the following section. A hysteresis controller is then used to control the DC-DC converter switches Q_1 or Q_2 to adjust the battery current i_{bat} (Fig. 8). In addition, the control signal is constrained within limits so that the actual charging/discharging current will be as per the specification of the battery and this will, eventually, enhance the the longevity of the battery. The inner current control loop is to force the battery current to follow the reference generated from the hysteresis control.

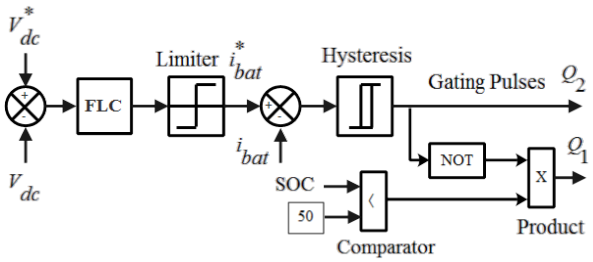

Figure 8: Overall structure of the battery controller

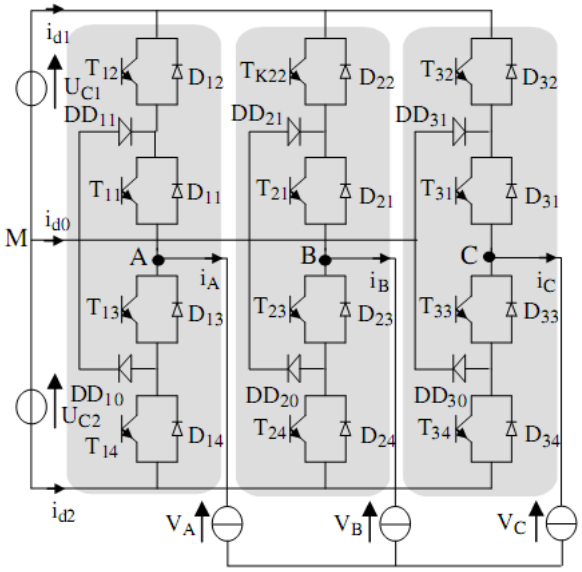

Figure 9: Topology of the three-level NPC converter

3. Modeling of the Three-Level NPC Inverter and Control Scheme

The topology of the three-level NPC converter is shown in Fig. 9. For the operation of this converter, five configurations are used. Table 3 presents the electrical magnitudes that characterize each configuration (with M as the origin of the potentials and V_{KM} ($K = A$, B or C) as the potential of node K of arm k ($k = 1$, 2 or 3)). The DC voltage sources U_{c1} and U_{c2} are provided by the rectifier (GSC). The modeling of a five-level NPC converter is discussed in more detail in [3, 5, 6, 25, 30–32, 34, 40].

3.1. Modeling of Intermediate Filter and Clamping Bridge Control

3.1.1. Model of the intermediate filter

The clamping bridge consists of a transistor in series with resistance, inserted to improve and stabilize the DC-voltage dynamic [41]. The intermediate filter scheme with clamping bridge is shown in Fig. 10.

The mathematical model of the intermediate filter is given by:

$$\begin{cases} C_1 \frac{dV_{C1}}{dt} = I_1 - I_{r1} - I_{d1} \\ C_2 \frac{dV_{C2}}{dt} = -I_2 - I_{r2} - I_{d2} \end{cases} \quad and \quad \begin{cases} I_{r1} = \frac{V_{C1}}{R_C} \\ I_{r2} = \frac{V_{C1}}{R_C} \end{cases} \tag{15}$$

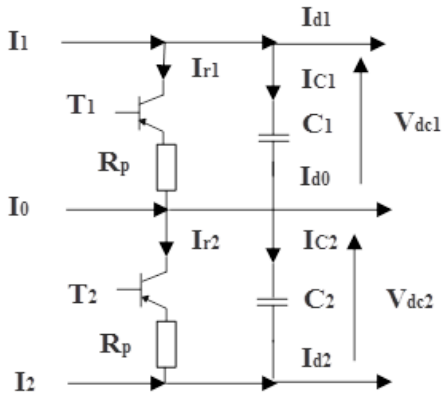

Figure 10: Intermediate filter structure with clamping bridge

3.1.2. Clamping bridge control

The control algorithm, which controls the clamping bridge, is applied separately for the upper and the lower stages. The algorithm compares, in real-time, the differences (ΔU_{12}) in the DC voltages of each stage to zero. If the difference is not equal to zero, the excess of energy will dissipate through resistance. The control algorithm of the clamping bridge is given as follows:

$$\begin{cases} \Delta V_{12} 0 \Rightarrow I_{r1} = 0 \;\&\; I_{r2} \neq 0 \; (T_1 = 0 \& T_2 = 1) \\ \Delta V_{12} 0 \Rightarrow I_{r1} \neq 0 \;\&\; I_{r2} = 0 \; (T_1 = 1 \& T_2 = 0) \end{cases} \tag{16}$$
$$\Delta V_{12} = V_{dc1} - V_{dc2}$$

3.2. Inverter Control

Pulse-width Modulation PWM converters for grid-integration of DG sources and their control strategies have been an ongoing research area over the last few decades [1, 6, 32, 34, 40, 42, 43]. The control strategy proposed in this paper is illustrated in Fig. 11 and consists of an outer power control loop for regulating the desired amount of power injection and an inner current control loop for controlling the current.

It is assumed that the grid supply and the output from a three phase VSC are ideal voltage sources. The load and voltage currents are transformed into the $\alpha - \beta$ reference as follows:

$$\begin{bmatrix} v_\alpha \\ v_\beta \end{bmatrix} = \sqrt{\frac{2}{3}} \cdot \begin{bmatrix} 1 & -\frac{1}{2} & -\frac{1}{2} \\ 0 & \sqrt{\frac{3}{2}} & -\sqrt{\frac{3}{2}} \end{bmatrix} \begin{bmatrix} v_a \\ v_b \\ v_c \end{bmatrix} \tag{17}$$

$$\begin{bmatrix} i_\alpha \\ i_\beta \end{bmatrix} = \sqrt{\frac{2}{3}} \cdot \begin{bmatrix} 1 & -\frac{1}{2} & -\frac{1}{2} \\ 0 & \sqrt{\frac{3}{2}} & -\sqrt{\frac{3}{2}} \end{bmatrix} \begin{bmatrix} i_a \\ i_b \\ i_c \end{bmatrix} \tag{18}$$

In the stationary reference frame and for a balanced three-phase system, the instantaneous active and reactive power outputs, seen from the network side, are obtained as:

$$\begin{cases} P = \frac{3}{2} \left(v_\alpha . i_\alpha + v_\beta . i_\beta \right) \\ Q = \frac{3}{2} \left(v_\beta . i_\alpha - v_\alpha . i_\beta \right) \end{cases} \tag{19}$$

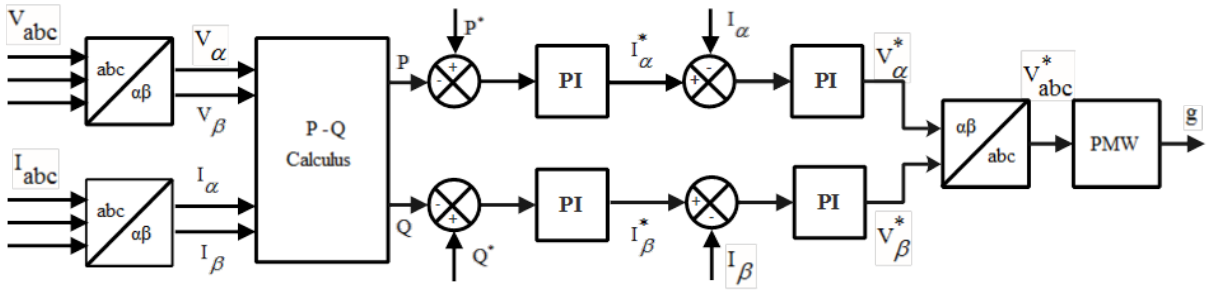

Figure 11: Proposed inverter control scheme

To achieve a unity power factor, a PI control loop is used to regulate the reactive power provided by the main grid to zero and provides the reference to the inverter.

4. Supervisory Control System

A supervisory controller was designed to manage the maximum energy captured from the grid and PV array. According to the flow chart shown in Fig. 12. In the first step, the supervisory controller compared the power generated and consumed. If the total power generated is greater relative to the power request, and if the battery is fully charged, the battery does not consume power from the PV and the grid decreases its production so as to provide stability between the power required and the power generated. If not, the battery consumes the difference in energy between the photovoltaic generator and load power.

If the total power generated is lower than the power request and if the photovoltaic power is nominal and if the SOC is greater to 20%, the battery provides the energy to the load to supplement the power delivered by the PV and grid. The battery power is often used to ensure stability of the DC voltage of the DC bus. Otherwise, the grid increases production to ensure stability and the grid ensures the production of energy for the power required.

5. Simulation Results And Discussions

In this article, the proposed control scheme used Fuzzy Logic Control (FLC) to control the DC voltage of a three level (NPC) inverter connected to the hybrid (PV-battery) system integrated into the grid. It is evaluated using MATLAB/Simulink software under variable load conditions. The proposed system parameters are listed in Table 1. The amount of power generated/supplied by the PV array depends on the solar irradiation $G = 1000$ W/m^2 and temperature $T = 293$ K. The proposed system is operated in three possible operating modes depending on the variable load. The system performance for this situation is shown in Figs. 13 to 19.

- Operating mode 1: when the grid and the PV generated the same powers to the load between $t = 0...0.5$ s Fig. 13 assuming the PV power generating system is greater than the difference between the load and the grid power ($P_{PV} \geq P_{Load} - P_{grid}$) and assuming the battery is not fully charged. The excess power of the PV array also simultaneously charges the battery bank, see Fig. 14.

- Operating mode 2: when ($P_{Load} \geq 0.11$ MW) the PV generated the nominal power to the load so the grid supplies power to the grid between $t = 0.5...1$ s Fig. 13, in this mode, the battery is able to provide power to ensure the stability of the DC-link voltage Fig. 14.

- Operating mode 3: when ($P_{Load} \leq 0.11$ MW) the grid supplies power to the grid between $t = 1...1.5$ s Fig. 13. In this mode, the PV panels can simultaneously supply tpower to the load, to the battery and to manage the DC-link voltage of the three-level NPC inverter Fig. 14.

The bi-directional buck/boost converter must have the ability to switch its operation between the boost and the buck mode, to be able to charge or discharge the battery power under variable load conditions.

These simulation tests provided insight into the effectiveness of the management approach taken and the various commands used. After obtaining the simulation results, we ensured equality between the power generated and sought for different loads applied to this hybrid system, which enabled stability to be achieved between the network and the renewable PV source with storage system.

Fig. 15 shows the wave forme of the grid current, PV current and load current respectively. In these Figures, we note that the current waveforms are sinusoidal and the frequency is maintained at 50 Hz.

Fig. 16 (a), (b) and (c) illustrate the zoomed of one phase of the grid voltage with the PV current, grid current and load current respectively. Fig. 16 (a) and (b) shows that the PV current and grid current are in π phase with the grid voltage, which implies that the PV and grid supply the active power. The grid current is in phase with the grid voltage Fig. 16 (c), which means that the load consumes energy from the grid and PV. We note that the amplitude of the grid voltage is constant, but the amplitude of the grid current and PV are variable depending on the variation of the load.

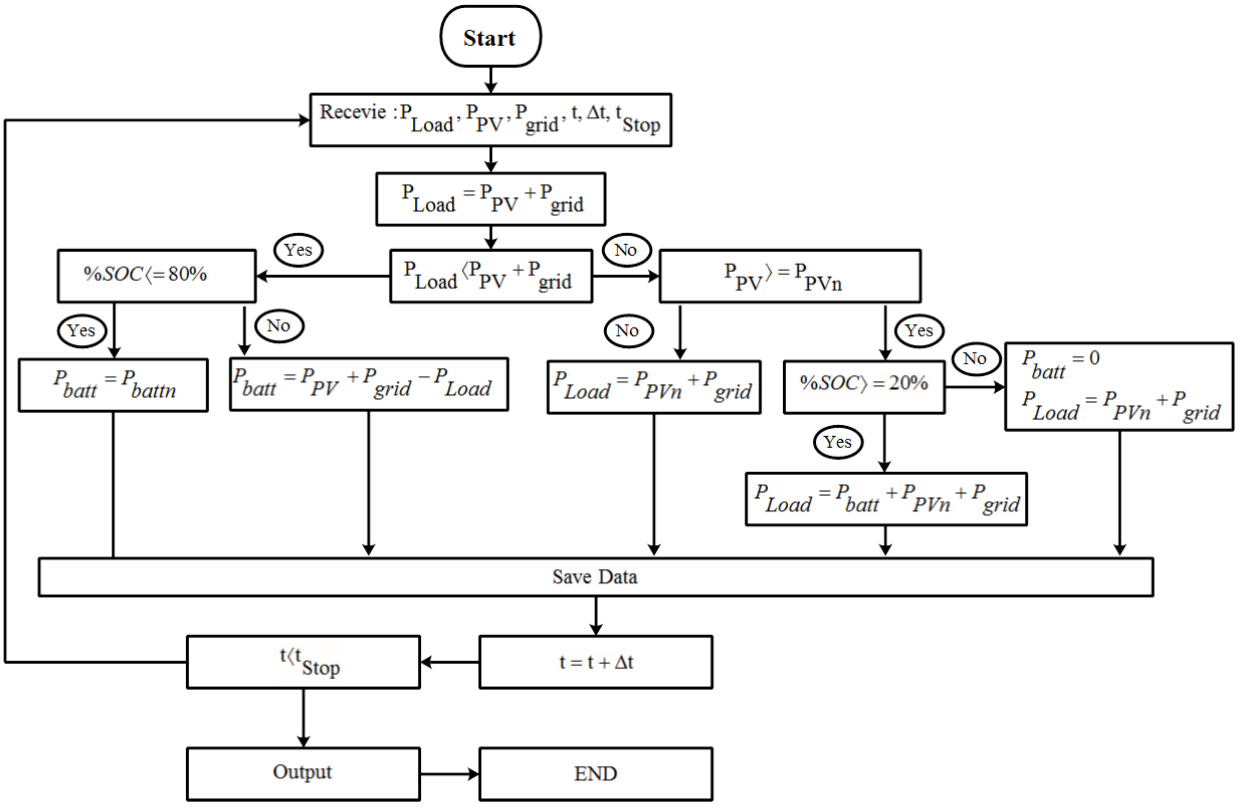

Figure 12: Flow chart of the supervisory controller

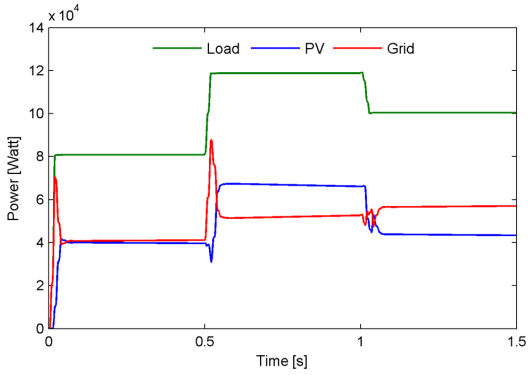

Figure 13: Distribution of the active power of: load (green), PV (blue), grid (red)

Fig. 17 shows that the measured DC voltage is successfully regulated at the reference value of 600 V. The proposed FLC control algorithm with clamping bridge circuit provides good control of the DC voltage. Fig. 18 confirms the balance and the stability of the neutral point. Furthermore, the Figure shows the differences between the DC voltages $(V_{dc1} - V_{dc2})$, which are kept null. This is due to the positive effect of the clamping bridge and its FLC control algorithm on DC voltage regulation.

Fig. 19 (a), (b) and (c) show the Total Harmonic Distortion (THD) analysis of the grid current, PV side inverter current and load current respectively for the load of 0.1 MW. The

Table 3: Total harmonic distortion for the proposed system

Load [MW]\THD [%]	0.08	0.12	0.1
Grid current	4.43	4.79	3.48
PV current	4.34	3.89	4.28
Load current	0.15	0.15	0.15

limits are those of international standards such as IEEE1547 (THD $<$ 5%). The THD for different load applied is given in Table 3. From this table we can clearly see that the THD for the three currents (grid, PV and load) has lower values, with 5% for different applied load (3 mode). We conclude that the use of the three-level NPC inverter for the hybrid (PV-battery) system integrated to the grid improves the quality of power in the system studied.

6. Conclusion

The article focused on the control strategy for a hybrid (PV-battery) system linked to the grid through a three-level NPC inverter. In this study, the PV array was connected to the DC bus through a boost converter to force the PV output to follow the maximum power. The DC bus then connected to the AC bus through a three-phase three-level DC-AC inverter. A DC-DC bidirectional converter connected between the DC-link and the battery was used to charge/discharge the battery.

The three level NPC inverter topology exhibits many advantages in terms of modularity, power quality, and capability of controlling each DC-link voltage separately. The FLC MPPT algorithm used features good tracking and efficiency performance while ensuring stable circuit operation. Various local control strategies were implemented to enhance the performance of the system, including regulation of the DC bus voltage. The proposed DC voltage control scheme consists of two loops: the outer closed loop controls the average value of the DC voltage by FLC, whereas the inner loop controls the difference between the two voltages in each half-arm, using a clamping bridge circuit. Various operating conditions were presented in simulation to evaluate the proposed management and control. The simulation results show that the proposed three level NPC inverter has demonstrated its ability to provide a high-quality injected current from the PV array into grid with a THD of less than 5%. We have provided stability of the DC bus voltage against variation of the load. These results show the efficiency of the management and the controls used for this hybrid system.

Acknowledgements

This work has been supported by Electrical Engineering and Informatics Engineering at the University Ibn-Khaldun (Tiaret-Algeria), with Polytechnic National School (Algiers-Algeria).

References

[1] P. Kakosimos, K. Pavlou, A. Kladas, S. Manias, A single-phase nine-level inverter for renewable energy systems employing model predictive control, Energy Conversion and Management 89 (2015) 427–437.

[2] N. Eghtedarpour, E. Farjah, Control strategy for distributed integration of photovoltaic and energy storage systems in dc micro-grids, Renewable energy 45 (2012) 96–110.

[3] K. Arulkumar, D. Vijayakumar, K. Palanisamy, Modeling and control strategy of three phase neutral point clamped multilevel pv inverter connected to the grid, Journal of Building Engineering 3 (2015) 195–202.

[4] A. Chouder, S. Silvestre, N. Sadaoui, L. Rahmani, Modeling and simulation of a grid connected pv system based on the evaluation of main pv module parameters, Simulation Modelling Practice and Theory 20 (1) (2012) 46–58.

[5] S. Ozdemir, N. Altin, I. Sefa, Single stage three level grid interactive mppt inverter for pv systems, Energy Conversion and Management 80 (2014) 561–572.

[6] N. Altin, S. Ozdemir, Three-phase three-level grid interactive inverter with fuzzy logic based maximum power point tracking controller, Energy Conversion and Management 69 (2013) 17–26.

[7] A. Oshaba, E. Ali, S. A. Elazim, Mppt control design of pv system supplied srm using bat search algorithm, Sustainable Energy, Grids and Networks 2 (2015) 51–60.

[8] T. Esram, P. L. Chapman, Comparison of photovoltaic array maximum power point tracking techniques, IEEE Transactions on energy conversion 22 (2) (2007) 439–449.

[9] F. Liu, S. Duan, F. Liu, B. Liu, Y. Kang, A variable step size inc mppt method for pv systems, IEEE Transactions on industrial electronics 55 (7) (2008) 2622–2628.

[10] Q. Mei, M. Shan, L. Liu, J. M. Guerrero, A novel improved variable step-size incremental-resistance mppt method for pv systems, IEEE transactions on industrial electronics 58 (6) (2011) 2427–2434.

[11] S. K. M. Niapour, S. Danyali, M. Sharifian, M. Feyzi, Brushless dc motor drives supplied by pv power system based on z-source inverter and fl-ic mppt controller, Energy Conversion and Management 52 (8) (2011) 3043–3059.

[12] M. Alata, M. Al-Nimr, Y. Qaroush, Developing a multipurpose sun tracking system using fuzzy control, Energy Conversion and Management 46 (7) (2005) 1229–1245.

[13] M. Ouada, M. Meridjet, M. Saoud, N. Talbi, Increase efficiency of photovoltaic pumping system based bldc motor using fuzzy logic mppt control, WSEAS Transactions on Power Systems 8 (3) (2013) 104–113.

[14] F. Aashoor, F. Robinson, Maximum power point tracking of photovoltaic water pumping system using fuzzy logic controller, in: Power Engineering Conference (UPEC), 2013 48th International Universities', IEEE, 2013, pp. 1–5.

[15] L. Letting, J. Munda, Y. Hamam, Optimization of a fuzzy logic controller for pv grid inverter control using s-function based pso, Solar Energy 86 (6) (2012) 1689–1700.

[16] M. Ouada, M. S. Meridjet, N. Talbi, Optimization photovoltaic pumping system based bldc using fuzzy logic mppt control, in: Renewable and Sustainable Energy Conference (IRSEC), 2013 International, IEEE, 2013, pp. 27–31.

[17] X. Feng, H. Gooi, S. Chen, Hybrid energy storage with multimode fuzzy power allocator for pv systems, IEEE Transactions on Sustainable Energy 5 (2) (2014) 389–397.

[18] H. Zhang, S. Cheng, A new mppt algorithm based on ann in solar pv systems, in: Advances in Computer, Communication, Control and Automation, Springer, 2011, pp. 77–84.

[19] M. A. Younis, T. Khatib, M. Najeeb, A. M. Ariffin, An improved maximum power point tracking controller for pv systems using artificial neural network, Przegląd Elektrotechniczny 88 (3b) (2012) 116–121.

[20] N. Altin, İ. Sefa, dspace based adaptive neuro-fuzzy controller of grid interactive inverter, Energy Conversion and Management 56 (2012) 130–139.

[21] A. Bahgat, N. Helwa, G. Ahmad, E. El Shenawy, Maximum power point traking controller for pv systems using neural networks, Renewable Energy 30 (8) (2005) 1257–1268.

[22] A. A. Kulaksiz, R. Akkaya, Training data optimization for anns using genetic algorithms to enhance mppt efficiency of a stand-alone pv system, Turkish Journal of Electrical Engineering & Computer Sciences 20 (2) (2012) 241–254.

[23] H.-T. Yau, Q.-C. Liang, C.-T. Hsieh, Maximum power point tracking and optimal li-ion battery charging control for photovoltaic charging system, Computers & Mathematics with Applications 64 (5) (2012) 822–832.

[24] D. Parra, G. S. Walker, M. Gillott, Modeling of pv generation, battery and hydrogen storage to investigate the benefits of energy storage for single dwelling, Sustainable Cities and Society 10 (2014) 1–10.

[25] K. Himour, K. Ghedamsi, E. M. Berkouk, Supervision and control of grid connected pv-storage systems with the five level diode clamped inverter, Energy Conversion and Management 77 (2014) 98–107.

[26] N.-K. C. Nair, N. Garimella, Battery energy storage systems: Assessment for small-scale renewable energy integration, Energy and Buildings 42 (11) (2010) 2124–2130.

[27] E. Rejovitzky, C. V. Di Leo, L. Anand, A theory and a simulation capability for the growth of a solid electrolyte interphase layer at an anode particle in a li-ion battery, Journal of the Mechanics and Physics of Solids 78 (2015) 210–230.

[28] S. Anuphappharadorn, S. Sukchai, C. Sirisamphanwong, N. Ketjoy, Comparison the economic analysis of the battery between lithium-ion and lead-acid in pv stand-alone application, Energy Procedia 56 (2014) 352–358.

[29] A. Salvadori, D. Grazioli, M. Geers, Governing equations for a two-scale analysis of li-ion battery cells, International Journal of Solids and Structures 59 (2015) 90–109.

[30] M. Abbes, J. Belhadj, New control method of a robust npc converter for renewable energy sources grid connection, Electric Power Systems Research 88 (2012) 52–63.

[31] G. Tsengenes, G. Adamidis, A multi-function grid connected pv system with three level npc inverter and voltage oriented control, Solar Energy 85 (11) (2011) 2595–2610.

[32] J. Alonso-Martı, S. Arnaltes, et al., Direct power control of grid connected pv systems with three level npc inverter, Solar Energy 84 (7)

(2010) 1175–1186.
[33] C. Bharatiraja, R. Palanisamy, S. S. Dash, et al., Hysteresis current controller based transformerless split inductor-npc-mli for grid connected pv-system, Procedia Engineering 64 (2013) 224–233.
[34] D. Lalili, A. Mellit, N. Lourci, B. Medjahed, C. Boubakir, State feedback control and variable step size mppt algorithm of three-level grid-connected photovoltaic inverter, Solar Energy 98 (2013) 561–571.
[35] A. Ravi, P. Manoharan, J. V. Anand, Modeling and simulation of three phase multilevel inverter for grid connected photovoltaic systems, Solar Energy 85 (11) (2011) 2811–2818.
[36] R. Shalchi Alishah, M. Barzegar, D. Nazarpour, A new cascade boost inverter for photovoltaic applications with minimum number of elements, International Transactions on Electrical Energy Systems 25 (7) (2015) 1241–1256.
[37] L. W. Yao, J. Aziz, P. Y. Kong, N. Idris, Modeling of lithium-ion battery using matlab/simulink, in: Industrial Electronics Society, IECON 2013-39th Annual Conference of the IEEE, IEEE, 2013, pp. 1729–1734.
[38] H. Beltran, M. Swierczynski, A. Luna, G. Vazquez, E. Belenguer, Photovoltaic plants generation improvement using li-ion batteries as energy buffer, in: Industrial Electronics (ISIE), 2011 IEEE International Symposium on, IEEE, 2011, pp. 2063–2069.
[39] M. M. Aly, E. Abdelkarim, M. Abdel-Akher, Mitigation of photovoltaic power generation fluctuations using plug-in hybrid electric vehicles storage batteries, International Transactions on Electrical Energy Systems 25 (12) (2015) 3720–3737.
[40] J. D. Barros, J. F. Silva, Optimal predictive control of three-phase npc multilevel converter for power quality applications, IEEE Transactions on Industrial Electronics 55 (10) (2008) 3670–3681.
[41] F. Merahi, E. M. Berkouk, Back-to-back five-level converters for wind energy conversion system with dc-bus imbalance minimization, Renewable Energy 60 (2013) 137–149.
[42] T. Noguchi, et al., A new three-level current-source pwm inverter and its application for grid connected power conditioner, Energy Conversion and Management 51 (7) (2010) 1491–1499.
[43] Q. Shi, H. Hu, W. Xu, J. Yong, Low-order harmonic characteristics of photovoltaic inverters, International Transactions on Electrical Energy Systems 26 (2) (2016) 347–364.

Nomenclature

a	Diode ideality factor
C	Input filter capacitance of PV converter
$I_{0,n}$	Nominal saturation current
I_0	Saturation current
I_{bat}	Battery current
I_{DC}	DC-link current
I_d	Diode current
I_{PV}	Photovoltaic current
$I_{sc,n}$	Nominal short-circuit current
K	Polarization voltage
K_I	Current coefficient
K_v	Voltage coefficient
L	Inductive filter
N_s	Cells connected in series
P	Real power
P_{bat}	Battery power
P_{Load}	Load power
P_{PV}	Photovoltaic system output power
Q	Reactive power
q	Electron charge
R	Conducting resistance
R_1, C_1	Effests caused by mass transport
R_2, C_2	Effests caused by the charge transfer
R_p	Parallel resistance
R_s	Series resistance
SOC	State of charge of the battery
T	Tempurature
V_α, V_β	Voltage in $(\alpha - \beta)$ reference
V_{bat}	Battery voltage
V_{DC}	DC-link voltage
$V_{oc,n}$	Nominal open circuit voltage
V_{PV}	Photovoltaic system output voltage
V_t	Thermal voltage

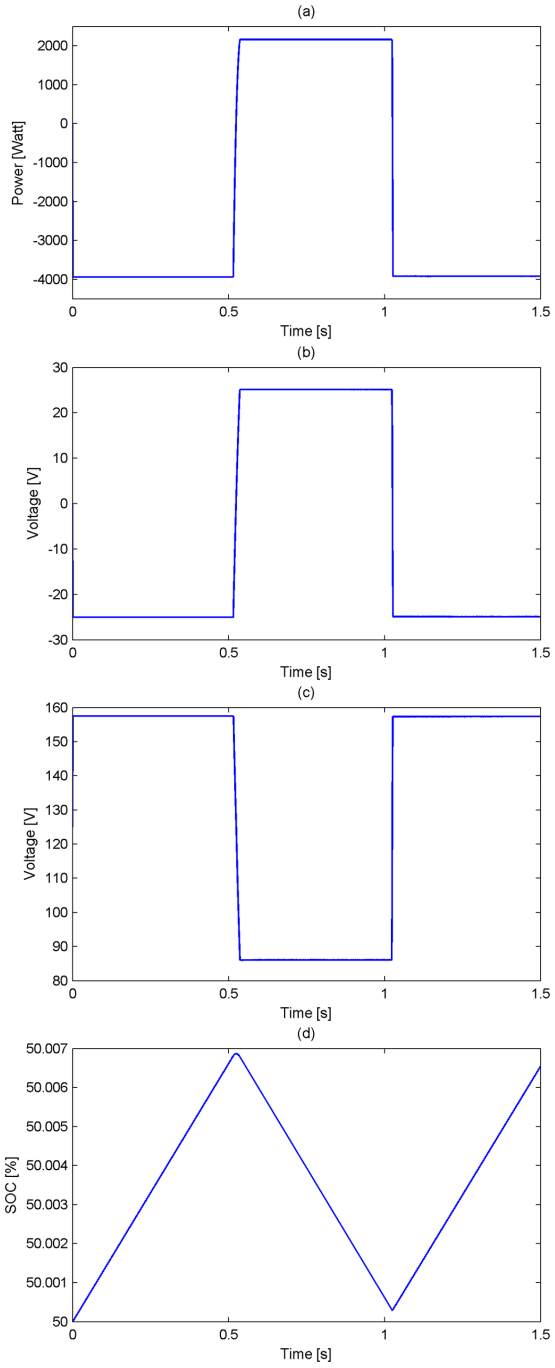

Figure 14: Battery response (a) Power (b) Current (c) Voltage (d) SOC

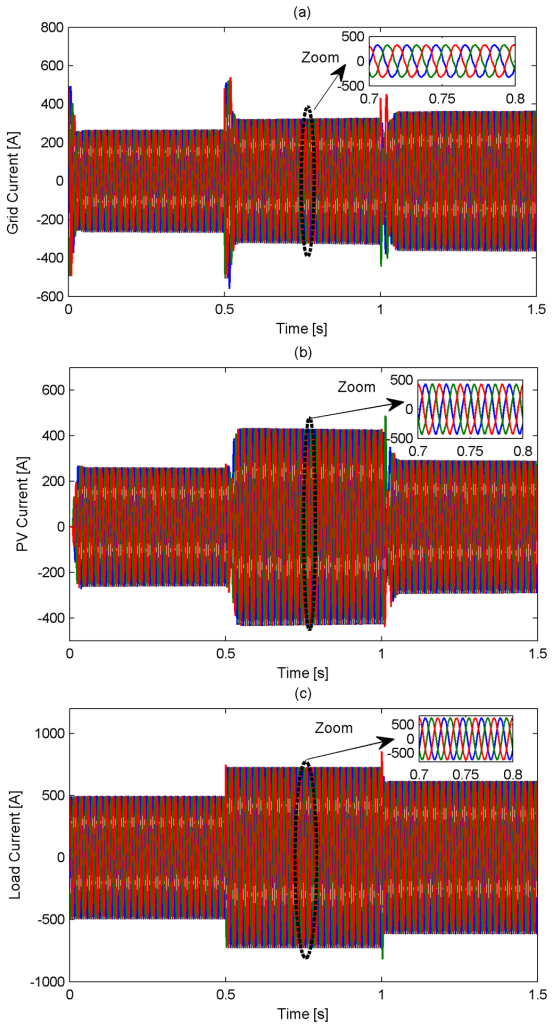

Figure 15: Waveforms currents: (a) Grid, (b) PV and (c) Load

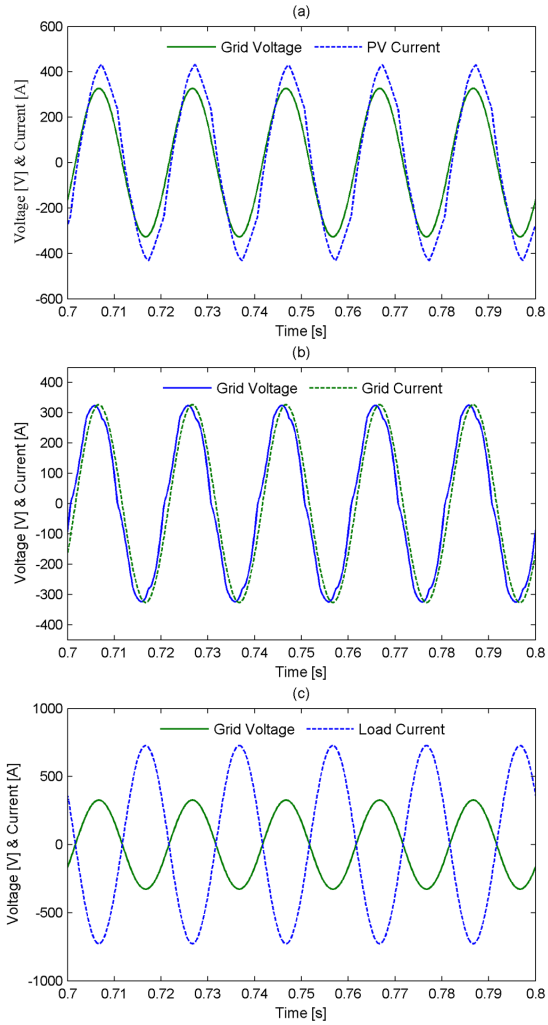

Figure 16: (a) Grid voltage and PV current, (b) Grid voltage and grid current, (c) Grid voltage and load current

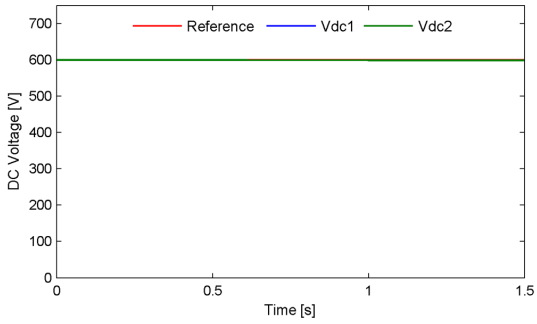

Figure 17: Average DC voltages

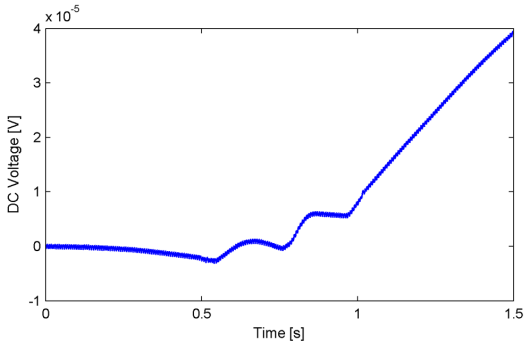

Figure 18: Voltage differences ($V_{dc1} - V_{dc2}$)

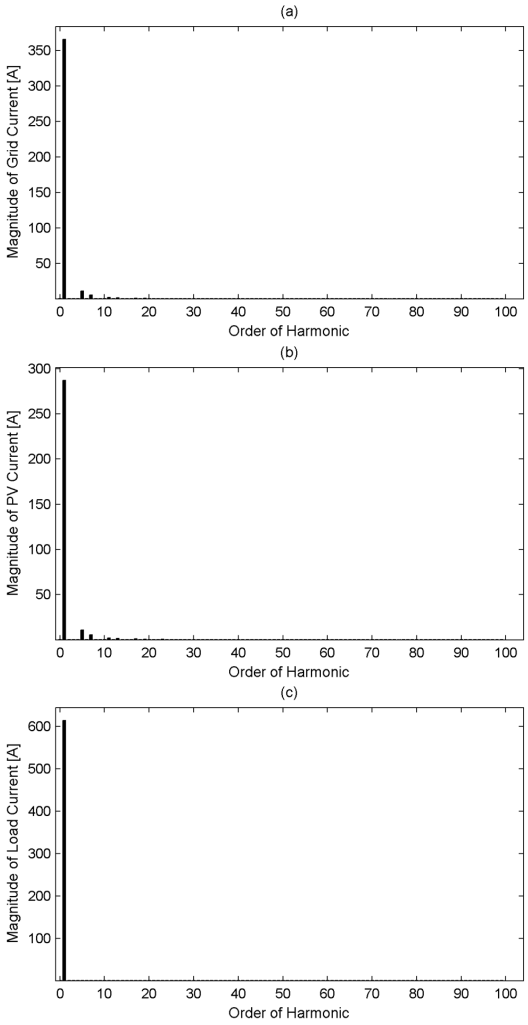

Figure 19: THD of current measurement for: (a) Grid current, (b) PV current, (c) Load current